JGR Solid Earth

RESEARCH ARTICLE
10.1029/2023JB026411

Lithosphere Structure, Processes, and Physical State of the Alpine-Apennine System

Irene Menichelli[1], Pasquale De Gori[2], Francesco Pio Lucente[2], Luigi Improta[2], and Claudio Chiarabba[2]

[1]Dipartimento di Scienze, Università degli Studi Roma Tre, Rome, Italy, [2]Istituto Nazionale di Geofisica e Vulcanologia, Rome, Italy

Key Points:

- Tomographic images of the central Mediterranean lithosphere/asthenosphere system with high lateral consistency and resolution
- The Alpine orogen is the result of the continuous underplating of the European plate
- The low *Vp* and high *Vp*/*Vs* anomalies show the presence of fluids below the chains correlated with extensional deformation at the surface

Supporting Information:

Supporting Information may be found in the online version of this article.

Correspondence to:

I. Menichelli and P. De Gori,
imenichelli@uniroma3.it;
pasquale.degori@ingv.it

Citation:

Menichelli, I., De Gori, P., Lucente, F. P., Improta, L., & Chiarabba, C. (2023). Lithosphere structure, processes and physical state of the Alpine-Apennine system. *Journal of Geophysical Research: Solid Earth*, *128*, e2023JB026411. https://doi.org/10.1029/2023JB026411

Received 12 JAN 2023
Accepted 4 APR 2023

Author Contributions:

Conceptualization: Irene Menichelli, Pasquale De Gori, Claudio Chiarabba
Data curation: Irene Menichelli, Pasquale De Gori, Francesco Pio Lucente, Luigi Improta
Formal analysis: Irene Menichelli, Pasquale De Gori, Francesco Pio Lucente, Luigi Improta, Claudio Chiarabba
Investigation: Irene Menichelli, Claudio Chiarabba
Methodology: Irene Menichelli, Claudio Chiarabba
Project Administration: Claudio Chiarabba
Supervision: Claudio Chiarabba

Abstract Tomographic images of the lithosphere are the first step to constrain the evolution of mountain belts and their interaction. By inverting new high-quality P- and S-wave arrivals that sample the entire lithosphere, we determined *Vp* and *Vp*/*Vs* models with reliable resolution in the critical depth range (40–80 km) where plates of the central Mediterranean area interact. This data set yields homogeneous representation of the 3D structure over a critical area at a regional scale. Here, we show that the Alps derive from a laterally continuous underthrusting of the European plate and that the Adria lithosphere was delaminated after the collision. Tomograms resolve the lateral changes of the continental versus oceanic subduction along the Alpine belt and identify original evidence of fluids beneath the orogens able to facilitate the current deformation.

Plain Language Summary A high resolution imaging of the lithosphere/asthenosphere system is crucial to understand tectonic processes of orogens and subductions. The Alpine chain is an exemplary case of complexity, with its lateral heterogeneity and changes. The largest seismic array ever developed in the Alpine chain (Alparray Seismic Network) has enabled the creation of a high-quality seismic data set contributing to new images of the entire central Mediterranean area. The novelty of this work lies in the enhanced resolution of velocity anomalies in a critical depth range (35–80 km) and with optimal homogeneity at the regional scale. The new 3D *Vp* and *Vp*/*Vs* models allow us to get insights into many open questions about the structure and evolution of the circum-Mediterranean orogens.

1. Introduction

The central Mediterranean is one of the most intriguing geodynamic areas in the world, ideal to test and improve the basis of plate tectonics. The interlaced circum-Mediterranean mountain belts result from the convergence between Africa and Eurasia coupled with the subduction of Tethyan oceanic realms (Faccenna & Becker, 2010). How the single systems evolved through time is known at the first order (Piromallo & Morelli, 2003; Wortel & Spakman, 2000), but plates interaction, subduction, and mountain belt formations are widely debated (Giacomuzzi et al., 2012; Lippitsch, 2003; Malusà et al., 2021; Paffrath et al., 2021; Zhao et al., 2016). The extreme complexity observed at the surface and testified by kinematics flourished the consolidation of different processes including continental delamination, slab break-off, and asthenospheric upwelling (Giacomuzzi et al., 2012; Wortel & Spakman, 2000). Here, we investigate the relationship between the Alpine and the Apennines belts, their architecture, and physical properties at lithospheric depth. An unsolved and intriguing topic concerns the nature of the slab beneath the Alps, Adriatic versus European in the Eastern Alps (i.e., Lippitsch, 2003; Schmid et al., 2004; Paffrath et al., 2021) and attached versus detached in the Western Alps (i.e., Handy et al., 2021; Lippitsch, 2003; Zhao et al., 2016). These issues have been discussed based on the different shape and geometry of the slabs revealed by tomographic models (Handy et al., 2021; Lippitsch, 2003; Mitterbauer et al., 2011; Paffrath et al., 2021; Piromallo & Morelli, 2003; Ustaszewski et al., 2008; Zhao et al., 2016). Debated interpretations also concern how the Alps evolution of the Alpine belt interacted with the slab retreat of the Apennines (Salimbeni et al., 2008; Thomson et al., 2010), and whether this last process is still ongoing or stalled (Carminati et al., 2012; Faccenna & Becker, 2010).

To address such big issues, we compute new *Vp* and *Vp*/*Vs* models for the central Mediterranean area by using manually picked P- and S-wave arrival times from 107 $M \geq 3.5$ earthquakes recorded by both permanent and temporary stations over a period of 5 years (Menichelli et al., 2022). We include data from the AlpArray temporary seismic project, the densest seismic array ever operating on a mountain belt (AlpArray Seismic Network, 2014;

Validation: Irene Menichelli, Claudio Chiarabba
Writing – original draft: Irene Menichelli
Writing – review & editing: Pasquale De Gori, Francesco Pio Lucente, Luigi Improta, Claudio Chiarabba

AlpArraySeismicNetwork, 2015; Hetényi et al., 2018). New data yield a decisive improvement in the definition of velocity structures emphasizing the homogeneity and consistency at a regional scale, on a depth range poorly defined so far (i.e., typically between 40 and 100 km depth, Handy et al., 2021), critical to make inference on the plate's interaction. We inverted high-quality Pg, Sg and long distance Pn, Sn observations by using the SIMULPS14 technique, progressively focusing on the lithosphere structure. We verified the model reliability through full resolution matrix analysis, checkerboard and restore tests. The velocity anomalies yield valuable information on the structure, composition, and thermal state of the lower crust-lithospheric mantle structure underneath the Alps and Apennines and allow us to propose new interpretations on the lithospheric processes, orogens interaction, and deep fluid circulation (Figure 1).

2. Data and Method

To produce a high resolution image of the lithosphere system, we have created a new high precision data set of P- and S- wave arrivals from moderate and large earthquakes ($M \geq 3.5$) recorded at local and regional scale. Arrivals have been read at a giant set of permanent and temporary stations including observations from the AlpArray project (AlpArray Seismic Network, 2014; AlpArraySeismicNetwork, 2015). A total of 42,584 arrival times (24,499 P- and 18,085 S-waves arrivals) from 107 earthquakes recorded by 1,679 seismic stations has been used and inverted (Figure 2). The number of stations and their spatial density is higher with respect to previous seismic investigation, allowing a finer sampling of the crust and the upper mantle. The applied selection of seismic events ensured a uniform distribution of the rays in the studied volume. The arrival times of both direct and refracted P- and S-waves at Moho (3,165 Pg, 21,334 Pn, 2,295 Sg, 15,790 Sn) were picked manually to reduce erroneous detection at large distances and to ensure high quality data. The Pn and Sn phases were read up to a maximum epicentral distance of about 1,000 km. Different weights based on accuracy and error estimation (0, 1, 2, 3) were assigned to each arrival time by the analysts. In addition, the polarity of the arrival time, upwards or downwards, was also defined. Absolute travel time residuals were computed using the 1D model (Menichelli et al., 2022; Figure 2c) as reference. The *Vp* and *Vp*/*Vs* and hypocentral parameters have been computed by using the linearized, iterative, damped least squares inversion method (SIMULPS14, Eberhart-Phillips & Reyners, 1997). Then, we compute the 3D velocity structure by using the damped least-square SIMULPS14 inversion code. Iterations are stopped when the variance improvement ceases to be significant. The damping value has been selected on the basis of the trade-off curve: the residual variance was plotted against the model norm. The chosen damping parameters of 1,000 for *Vp* and 1,400 for *Vp*/*Vs* are updated at each iteration. We followed a multistep procedure for the 3D model inversion.

- Step 1: A first coarse 3D *Vp* and *Vp*/*Vs* model has been computed on a 3D grid of nodes spaced $50 \times 50 \times 10$ km. In this step, all seismic phases with a residual time $\leq$4 s and a maximum epicentral distance from the stations of 900 km were inverted. Seismic events were treated as blasts, so they were inverted only for their time of origin; meanwhile, the position was kept fixed. The use of earthquakes as blasts is reasonable because of the good starting locations and the small shift in hypocentral parameters a posteriori observed (in step 2) after relocation (see Supporting Information), leading to small changes in arrival times with respect to velocity perturbations over long ray paths. After three iterations, we achieve a variance improvement of 46.24% and a final RMS of 0.726.
- Step 2: the seismic events have been relocated in the above-mentioned best-fitting 3D velocity model by using a maximum of 600 observations for each event, a residual time value $\leq$3 s, and a maximum epicentral distance of 400 km (see Supporting Information).
- Step 3: We compute a fine model with a $25 \times 25 \times 10$ km grid of nodes, by using the coarse model as the starting model for depths greater than 30 km. The *Vp* and *Vp*/*Vs* model is computed at the fine scale only for depths less than 35 km, by using only phase data with a maximum epicentral distance of 400 km and four iterations with a simultaneous inversion for velocity and hypocentral parameters. After four iterations, the variance improvement achieved has been 41.68% with a weighted RMS residual of 0.626 (variance ratio and critical ratio = 1.0119 and 1.003).

The hypocentral adjustments and errors have been analyzed for all coordinate components: *x*, *y*, and *z* (see Supporting Information). The values of the estimated hypocentral errors are less than 1 and 2 km for the horizontal and vertical components, respectively. A few earthquakes have larger errors but we keep these events since they enhance the ray sampling within the target volume.

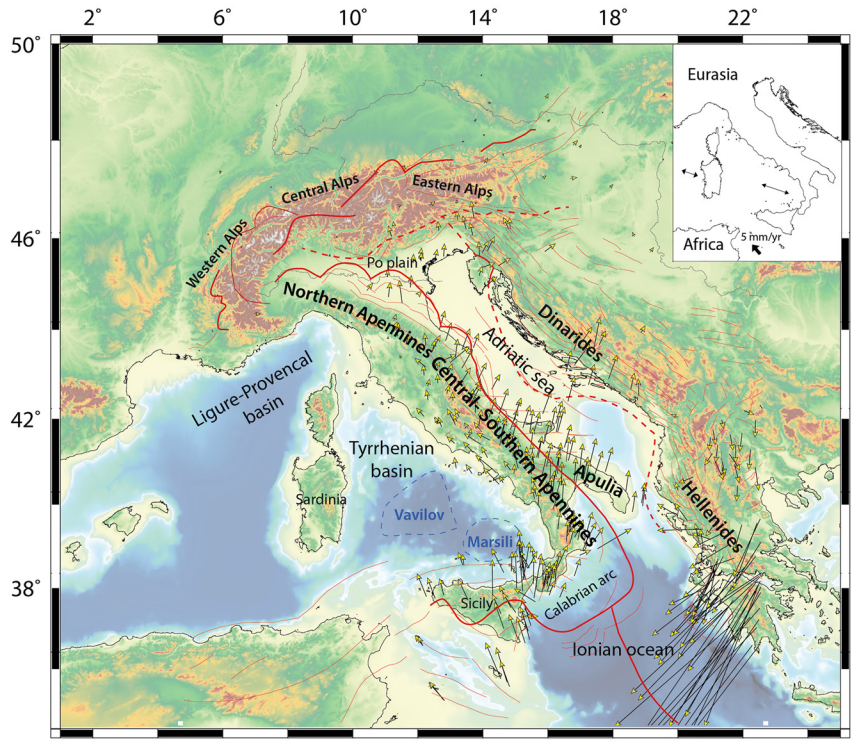

Figure 1. Map of the central Mediterranean area with the main lineaments modified from Faccenna et al. (2014) and the present surface motions extracted by Nocquet (2012).

2.1. Resolution Analysis

The reliability of our tomographic model has been accomplished by the analysis of the complete resolution matrix and by performing a checkerboard, a restore and a specific synthetic test (Figures 3–5). The resolution matrix has been analyzed through a quantitative inspection of each averaging vector that is performed by computing the Spread Function (SF hereinafter; Michelini & McEvilly, 1991). For each inverted node, SF is computed accounting for the diagonal element of the averaging vector while weighting the off diagonal elements (i.e., the contribution of the remaining nodes) with the euclidean distance from the considered node. Therefore, for a well resolved node, SF tends to be small since the averaging vector is numerically dominated by the diagonal element of the resolution matrix. Conversely, the quality of resolution decreases (large SF) when the averaging vectors are characterized by large off-diagonal values. To establish the threshold of SF above which resolution degrades, we analyzed for all the model parameters the correlation between SF and node ray sampling quantified by the Derivative Weight Sum (DWS). In a two dimensional plot, DWS and SF describe a L-shape trend with DWS that decrease for increasing SF values. Following Toomey and Foulger (1989), the upper threshold of SF that ensures the best resolution should be chosen at the kink of observed L-shaped trend. For this tomographic study we select a SF limit of 2.0 for *Vp* and *Vp*/*Vs* models. Furthermore, the analysis of smearing distribution (see Figure S9 in Supporting Information S1) indicates that for $2 >> SF \leq 2$ the smearing effects are concentrated around the nodes, demonstrating that the selected SF limit ensures the compactness of averaging vectors.

To further assess the resolution of the tomographic features in the lower crust and mantle, and define the sensitivity of the model on the spatial length of the real structure (Lévěque et al., 1993), we computed three different synthetic tests (Figures 3–5). In the first test, the synthetic model that we try to reproduce is the real model of the inversion. For the checkerboard test, the synthetic model consists of alternated ±5% of anomalies with spatial length of 75 km in the *x* and *y* direction and 10 km along depth (Figure 5). In a third test, we simulate two continuous high *Vp* (+5%) and low *Vp*/*Vs* (−5%) slabs underneath the Alps and Apennines in the uppermost mantle (Figure 4). Then, travel times were calculated in the synthetic velocity model using the same sources and seismic stations configuration as in the original inversion. Finally, the synthetic arrival times were inverted, after adding Gaussian random noise, starting from the 1D model and adapting damping parameters, to test the ability

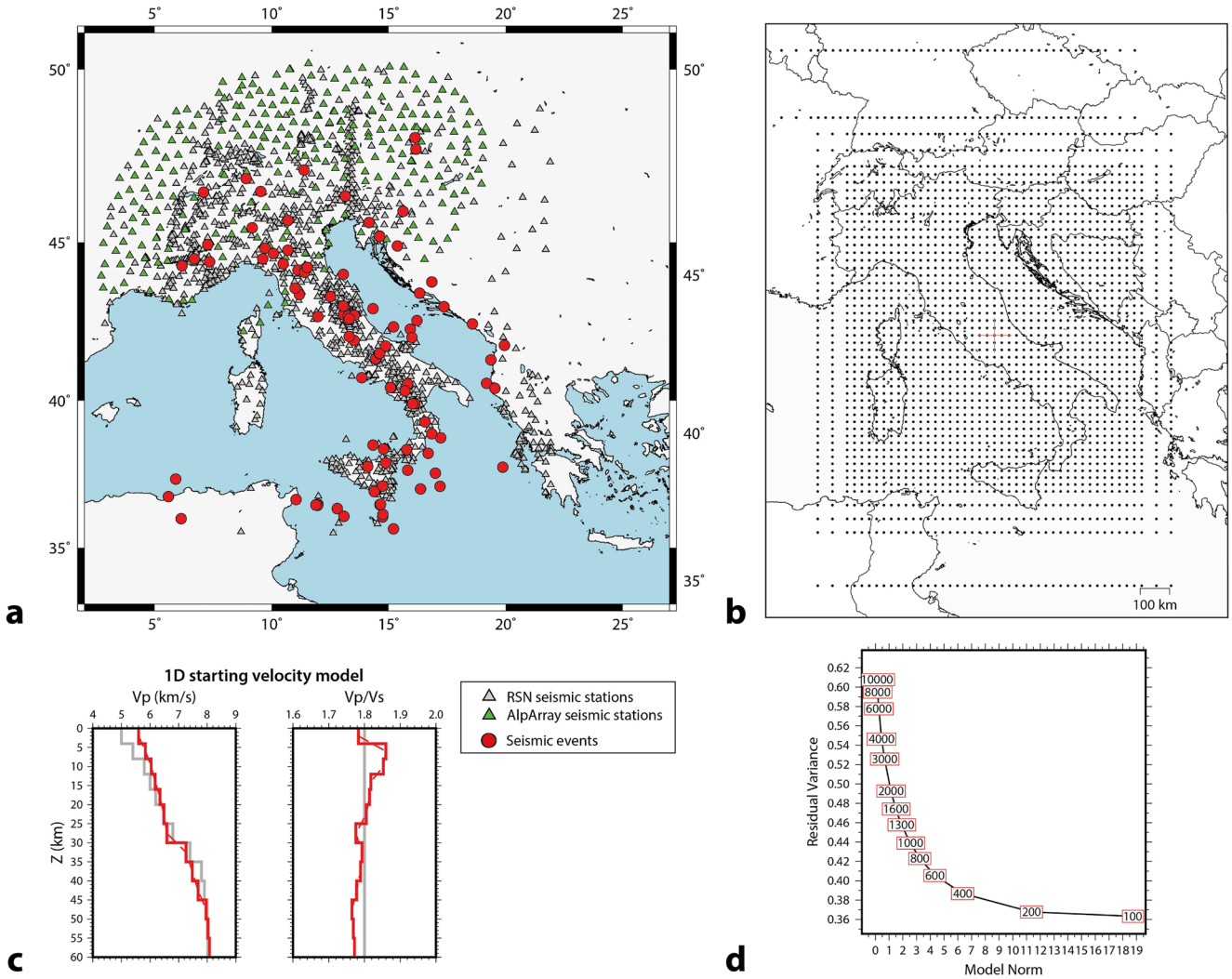

Figure 2. (a) Red dots indicate the 107 seismic events inverted to calculate the 3D tomographic model. The green and gray triangles indicate the AlpArray and RNS (i.e., National Seismic Network) seismic stations, respectively. (b) The grid of nodes (25 × 25 × 10 km) used to calculate the model. (c) The starting (gray line) and final (red line) 1D *Vp* and *Vp*/*Vs* models by Menichelli et al. (2022) used in the inversion procedure. (d) The trade-off curve calculated to set the damping parameters on *Vp* values with SIMULPS14.

to recover the synthetic model. The results of the three tests give us inferences on the spatial length of anomalies that could be resolved and thus the model sensitivity, showing the eventual smearing of anomalies in the volume and addressing, along with the SF, the model reliability. The recovery of synthetic features is reasonably good in the crust and good in the mantle, indicating that the anomalies modeled from 35 to 60 km depth are highly reliable (Figures 3–5).

3. Results: Lithosphere Structure of the Alps and Apennines

Figure 6 shows the *Vp* and *Vp*/*Vs* models, where well-resolved areas are delimited by a purple contour line (i.e., resolution is 70% of the diagonal element) according to the resolution analysis. Intense lateral heterogeneities are evident from the upper to the lower crust, in part consistent with previous studies (Di Stefano & Ciaccio, 2014; Di Stefano et al., 2009; Scafidi et al., 2009; Scafidi & Solarino, 2012). To interpret the *Vp* and *Vp*/*Vs* models in terms of lithology and rock physical properties (e.g., fracturing, hydration, fluid content), we used literature information. For crystalline rocks, we considered compilations of laboratory measurements of P-wave and S-wave velocities for lithologies of the continental and oceanic lithosphere (Christensen, 1996, 2004), focusing on subduction-related settings (Bezacier et al., 2010; Grevemeyer et al., 2018; Reynard, 2013). Regarding the upper

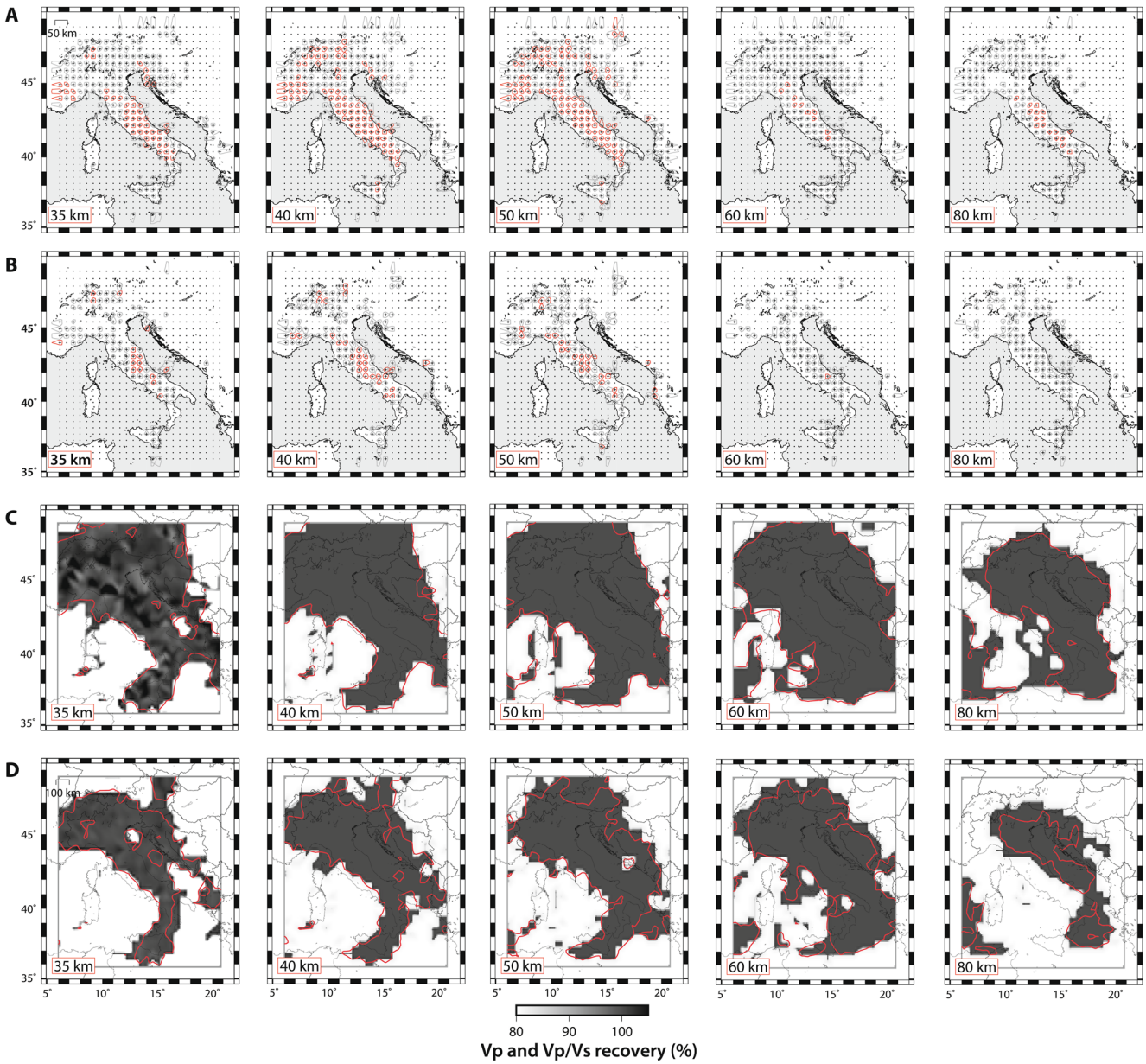

Figure 3. On top, Spatial distribution of 70% smearing contour for nodes of *Vp* (a) and *Vp*/*Vs* (b) model (35–80 km) layers (similar maps for all the other layers are reported in the supporting information). The nodes with SF (i.e., Spread Function) <2.0 are in red and with 2.0 < SF < 3.0 are in black. On the bottom, % velocity recovered from the recovery test for the *Vp* (c) and *Vp*/*Vs* (d) layers (35–80 km) of the computed 3D tomographic model. The red contour lines indicate where the resolution is 70% of the diagonal element.

crust, we considered laboratory and well logs measurements of P-wave and S-wave velocities for sedimentary rocks and low-grade metasediments of the Apennines belt and Padano-Adriatic-Apulian domains (Bally, 1987; Improta et al., 2003; Trippetta et al., 2010), as well as results of studies combining local earthquake tomography with hydrocarbon exploration data (Buttinelli et al., 2018; Chiarabba et al., 2014; Improta et al., 2017). The Alpine crust is characterized by *Vp* and *Vp*/*Vs* anomaly patterns variable with depth. High *Vp* and very-low *Vp*/*Vs* dominate in the uppermost 10 km (Δ *Vp* $\sim$ 5%, Δ *Vp*/*Vs* down to -5%), whereas low-*Vp*, low-*Vp*/*Vs* weak anomalies prevail in the mid-crust. These anomalies, corresponding to *Vp* of 6.0–6.3 km/s and *Vp*/*Vs* around 1.75, suggest the prevalence of felsic rocks in the crystalline mid-upper crust (Christensen & Mooney, 1995). The high *Vp* Ivrea-Verbano body clearly emerges and its rooting within the Adria (AM) mantle is evident (Figures 6 and 8a). Along the outer Apennines and to the north of the Alps, low-*Vp* upper-crustal anomalies relate to the

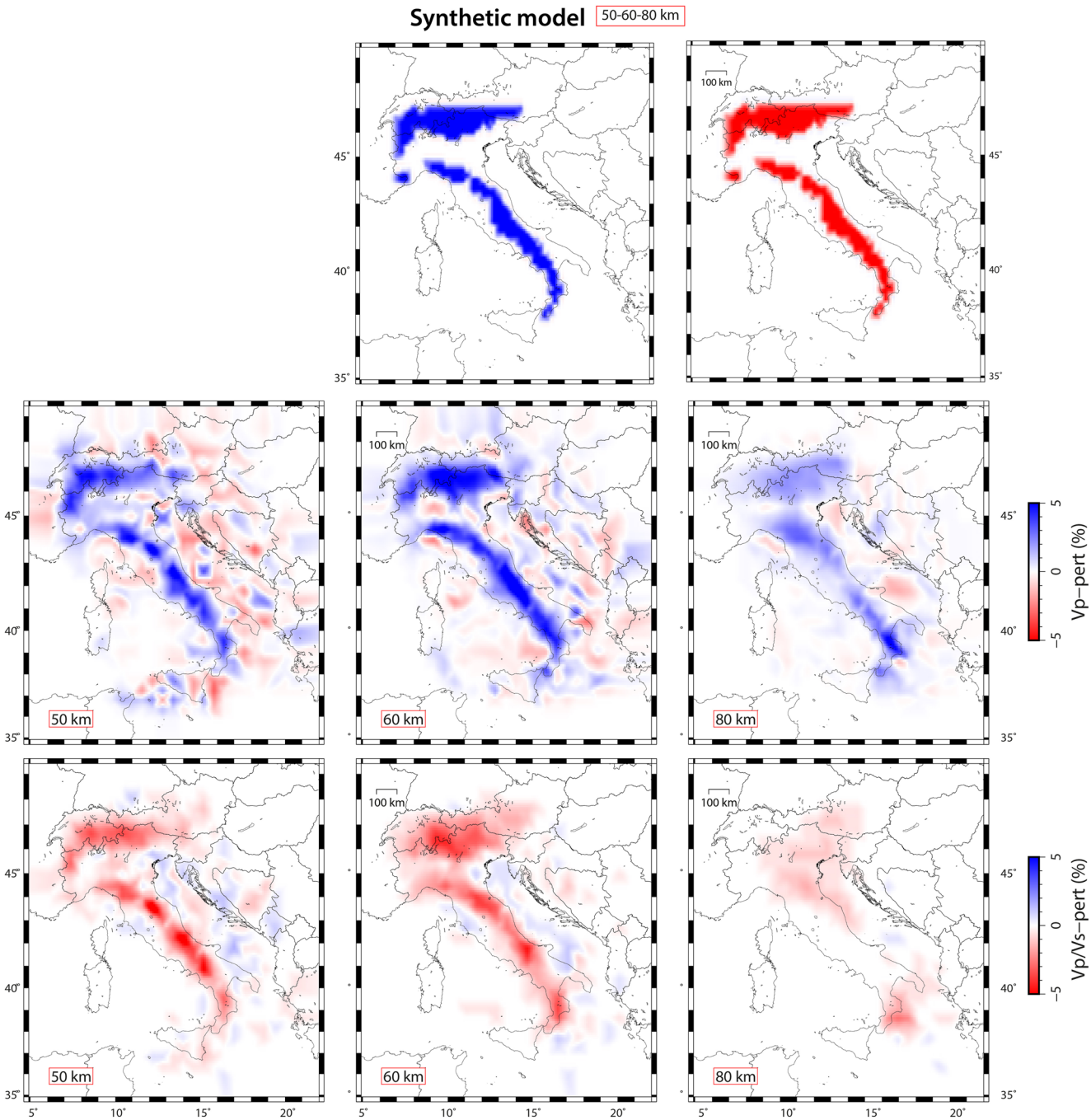

Figure 4. Synthetic test results where two continuous high *Vp* (+5%) low *Vp*/*Vs* (−5%) slabs underneath the Alps and Apennines in the uppermost mantle (50–80 km) have been simulated.

Padano-Adriatic-Apulia and Molasse foreland basins, respectively (Figures 8 and 9), while high *Vp*, high *Vp*/*Vs* anomalies correspond to carbonate units of the Apennines range and Adriatic-Apulia foreland (Chiarabba et al., 2014; among others). This trend is still present at mid-crustal depth, and the less intense and negative anomalies might indicate the presence of an acid-granitic crust, consistent with the continental nature of the Adria margin. At 30 km depth, the boundary between the Adriatic, European and Ionian Moho is easily identified by the sharp contrasts between high and low *Vp* anomalies, consistent with regional studies. In particular, the transition between low-velocity anomalies under the axial-outer zones of Apennines and high-velocity anomalies under its Tyrrhenian side follows the boundary between the Adriatic and Tyrrhenian plates (Spada et al., 2013).

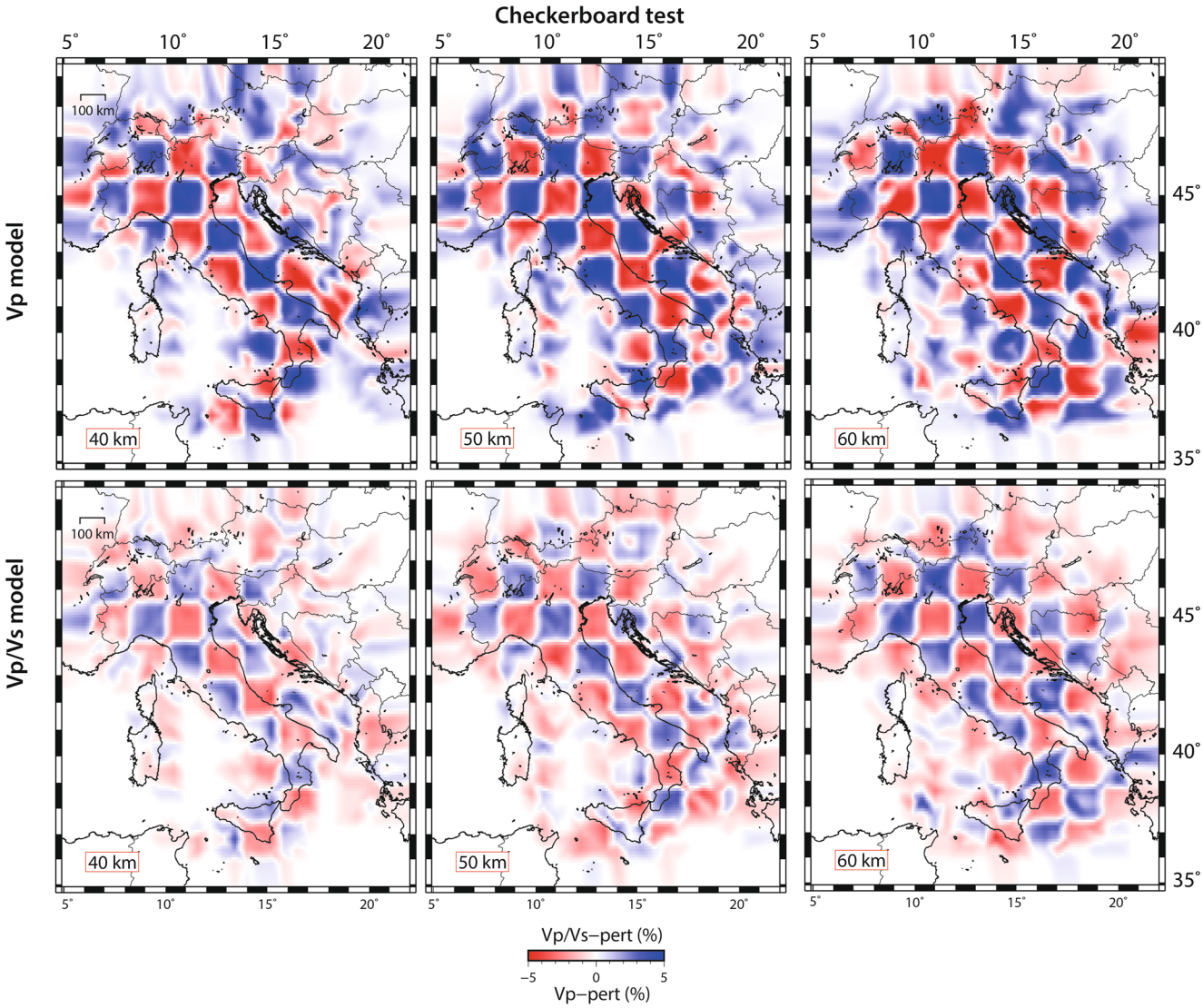

Figure 5. Checkerboard test results for the *Vp* and *Vp/Vs* 40, 50, 60 km layers. The synthetic model consists of alternated ±5% of anomalies with spatial length of 75 km in the *x* and *y* direction and 10 km along depth.

Another interesting feature is the low *Vp*/*Vs* below the southern part of the Dora Maira massif that becomes below 25–30 km a high *Vp*/*Vs* anomaly. The location of this body leads us to link to the Ivrea body (see Figure 6), well visible also in the cross-section (Figures 7 and 8a). The switch from low to high *Vp*/*Vs* defines the transition between the European lower crust and the Adria mantle wedge, where the Ivrea body is rooted, in agreement with past studies (Diehl et al., 2009).

Below the Moho depth (>40 km), high *Vp* and low *Vp*/*Vs* anomalies describe the European (EM), Adriatic (AM) and Ionian (IM) lithospheric mantle. The high (Δ *Vp* < 5%), low *Vp*/*Vs* anomaly of the EM plunges southward along the entire Alpine belt. Sandwiched between the EM and AM, the central deep portion of the Alpine belt is marked by an extended low *Vp* (Δ *Vp* < −5%) and high *Vp*/*Vs* (Δ *Vp*/*Vs* > 2%) arc-shaped anomaly with an ENE-WSW trend that spreads to the Vienna Basin, and the Dinarides. This anomaly narrows down to 60 km depth, where the EM and AM high Vp anomalies are welded (sections (b) and (c) of Figure 8). At 60–80 km depth, the AM is clearly defined plunging beneath the Apennines (Figure 6). Although the general feature of the AM is a high velocity, spots of low *Vp* and low *Vp*/*Vs*, that is, high Versus, suggest the presence of compositional anomalies in the AM mantle. This pattern, with a change from positive to negative anomalies north and south of 42°N, is evident at 60 km depth, identifying a main heterogeneity in the Adria plate. At a broad scale, the high

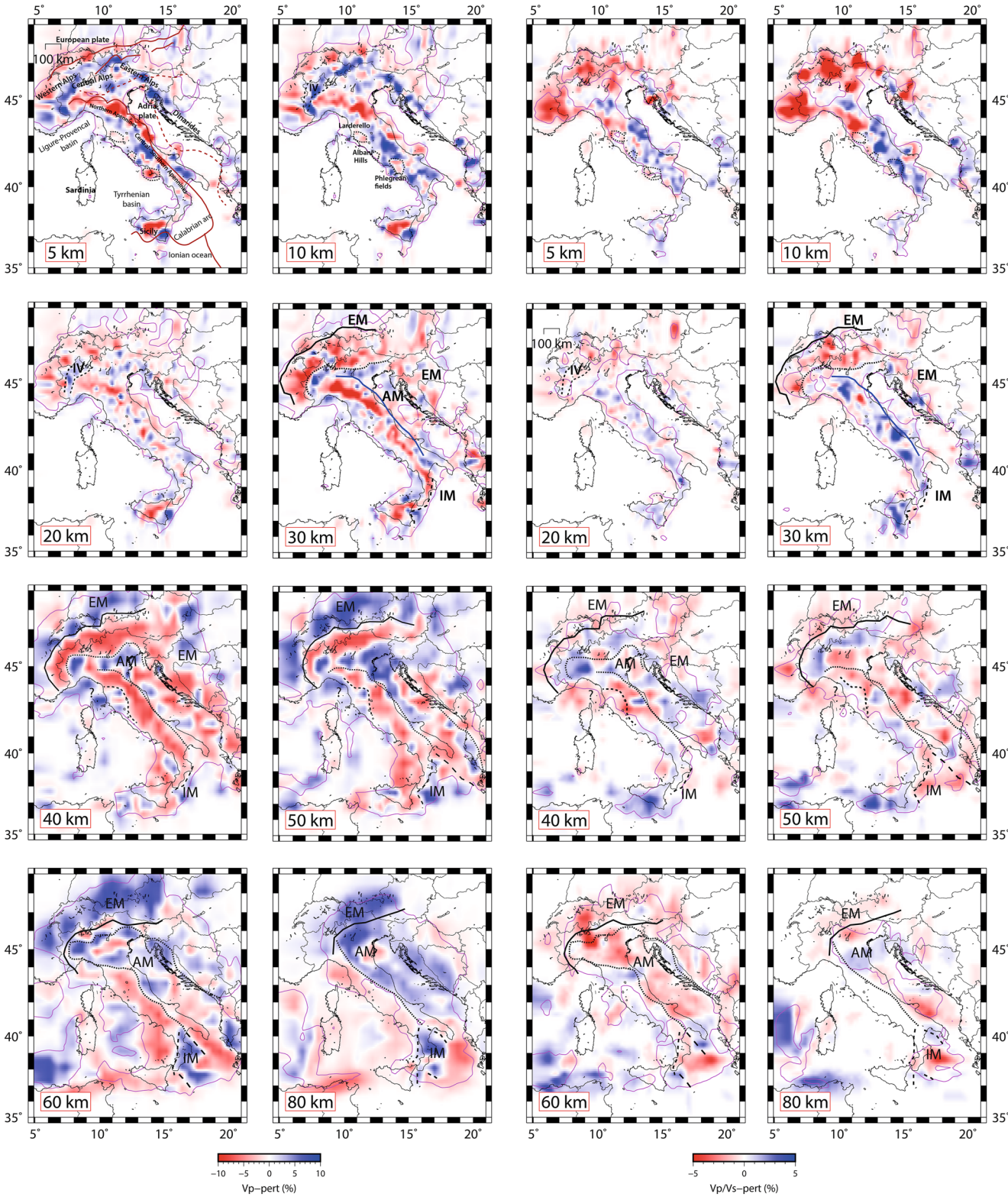

Figure 6. *Vp* pert and *Vp*/*Vs* pert (%) (left and right panel) models in layers between 5 and 80 km. The purple lines indicate where the resolution is 70% of the diagonal element. The black lines shown in the velocity layers highlight the depth of the Adriatic, European, and Ionian lithospheric mantle and are plotted following using as a proxy the abrupt change from the low perturbation *Vp* zones (+%) to higher perturbation *Vp* zones (−%). At 30 km depth, the blue line is the moho depth in agreement with Spada et al. (2013) moho map.

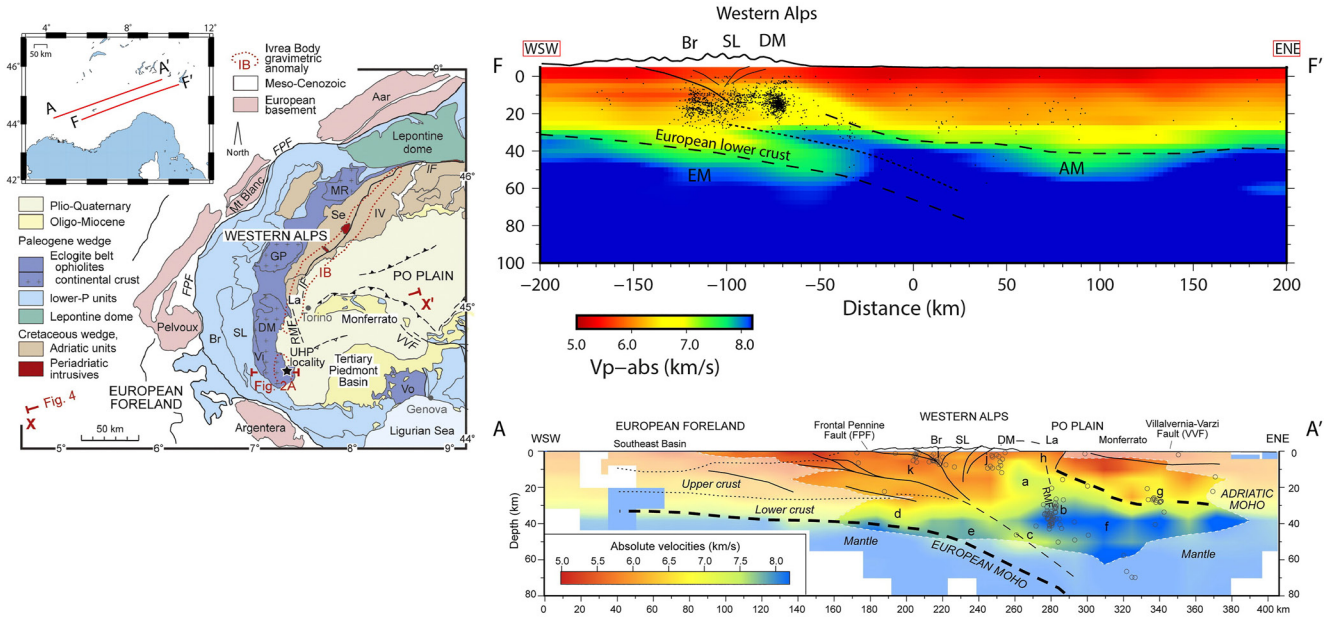

Figure 7. *Vp* absolute tomographic section crossed the western Alps (F–F′). The top left map (modified by Solarino et al. (2018)) shows the location of the profile. On top right the profile in the map is reported. A direct comparison with the one of section A–A′ of Solarino et al. (2018) is reported in figure. EM = European lithospheric mantle, AM = Adriatic lithospheric mantle, BR= Brianconnais zone, SL= Sesia-Lanzo DM = Dora Maira Massif.

Vp Adria plate is defined, colliding in the Alps and subducting in the Apennines and Dinarides. The Apennines are marked by a strong NNW-SSE low *Vp* anomaly ($\Delta\ Vp < -5\%$) at 40–60 km depth, which follows the characteristic trend of the chain. To the east, the boundary with the high *Vp* anomaly marks the position of the Adria plate. Its westward dip sectors is highlighted by the shift of this positive anomaly ($\Delta\ Vp > 2\%$). Below the northern Apennines, this anomaly turns out to be connected with the high-velocity anomaly residing below the inner Alps. The Ligurian and northern Tyrrhenian basins are represented by a high *Vp* and low *Vp*/*Vs* anomaly ($\Delta\ Vp/Vs < -1/-2\%$) at 40–50 km depth. While the Ionian area is characterized by a well-defined high *Vp* and low *Vp*/*Vs* anomaly at 50 km depth that marks the Ionian oceanic lithospheric mantle. At depth, it becomes broader and stronger, dipping northwestward beneath the Calabrian Arc highlighting the subducted Ionian plate (Figure 6). A distinctive high *Vp*/*Vs* anomaly is present in the mantle wedge sandwiched between the high *Vp* Ionian lithosphere and a high-*Vp* anomaly at 20–30 km that is related to the Tyrrhenian lithospheric mantle (Figures 6 and 9). Below the northwestern side of Sicily and the Aeolian Island, a low *Vp* and a high *Vp*/*Vs* anomaly ($\Delta\ Vp/Vs > 2\%$) is present at 40–50 km depth. The resolution is limited at greater depth and the anomalies are weak.

4. Comparison With Previous Tomographic Studies

We compared the main resolved features in the layers between 35 and 60 km (where the highest resolution was reached, see Figures 3–5), with the velocity models presented in literature (Di Stefano & Ciaccio, 2014; Di Stefano et al., 2009). At a large scale, the gross *Vp* pattern coincides with previous models (Di Stefano et al., 2009). The inner part of the Alpine chain and the Adriatic side of the Apennines are characterized by a large low *Vp* anomaly interrupted by some high *Vp* pulses, whilst the Ligurian Sea is characterized by a high *Vp* anomaly. However, if we compare the location, the details, and amplitudes of velocity anomalies, we note some main differences. For example, the positive anomaly marking the Ligurian Sea up to 50 km in our *Vp* model appears smaller in the 52-km layer of Di Stefano et al. (2009) where it is more shifted southward, and much different from the strong low *Vp* anomaly in Di Stefano and Ciaccio (2014). We observe a similar low *Vp* anomaly at greater depths (60–80 km). At 40–50 km depth, our model recovers a high velocity anomaly under the Western Alps in the same area where Di Stefano et al. (2009) defined a low velocity body. The Tyrrhenian Sea is characterized by a low-velocity anomaly interrupted by a higher one at 39°N, 15°E that in Di Stefano's 38-km depth layer appears to be larger, expanding southwestward along the Sicilian coast. At 50–52 km depth, the two models again coincide, showing a large low-velocity anomaly related to the presence of asthenospheric material. In our model, the

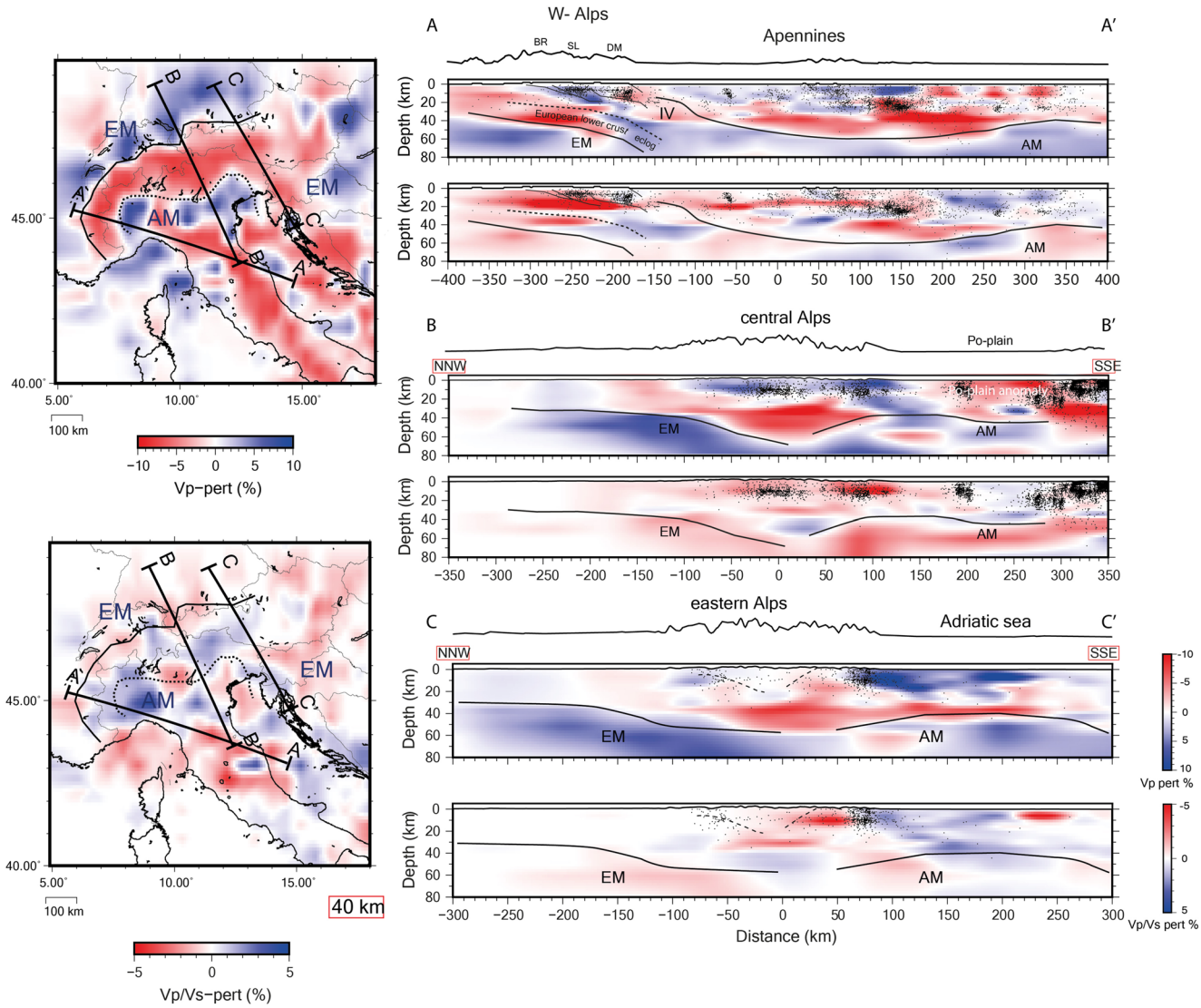

Figure 8. On the left, *Vp* and *Vp/Vs* layers at a depth of 40 km with the traces of the sections (black lines) shown on the right, with the relative seismicity (2005–2012, Chiarabba et al., 2015). The structure of the Western (A–A′), Central (B–B′), and Eastern Alps (C–C′) has been well reconstructed showing the southward underplating of the European plate with no evidence of a change in plate polarity. Black lines indicate the Adriatic (AM) and European lithospheric Mantle (EM) and dotted lines indicate a position that is not highly constrained. BR= Brianconnais zone, SL= Sesia-Lanzo DM = Dora Maira Massif.

Sicilian area is well resolved down to 60 km depth, whilst in the *Vp* model of Di Stefano et al. (2009) the resolution is lost below 52 km depth. Significant differences in the *Vp* model can be observed along the Adriatic coast, between the Apennines and the Dinarides. The high *Vp* anomaly extending between 42 and 45°N and 15–20°E along the Adriatic is narrower in our model, not also involving the eastern side of the Apennine chain as in Di Stefano's models. A huge low *Vp* anomaly covers the Calabrian arc and the southern Adriatic at 40–60 km only partly recovered by past velocity models as in that of Di Stefano and Ciaccio (2014) (see layers at 52 km depth in Figure 7). As a whole, the resolution at depth larger than 40 km is higher in our model thanks to the addiction of long traveling Pn and Sn arrivals. Our model also emphasizes small details of the lithosphere.

In Figure 7, we compared the velocity structure of the Western Alps with that recovered from the model of Solarino et al. (2018). The main features appear similar in geometry and absolute velocity values. The descent of the European lithosphere beneath Adria is clearly visible. In both models, the European lower crust is characterized by velocities ranging from 6.5 to 7.8 km/s, while the upper layers show lower velocity values of 5.0–6.2 km/s. Similar values also characterize the Adria crust, whose boundary with the mantle lithosphere appears rather horizontal toward the northeast, whilst below the Western Alps it becomes shallower pushed upward by the mantle wedge.

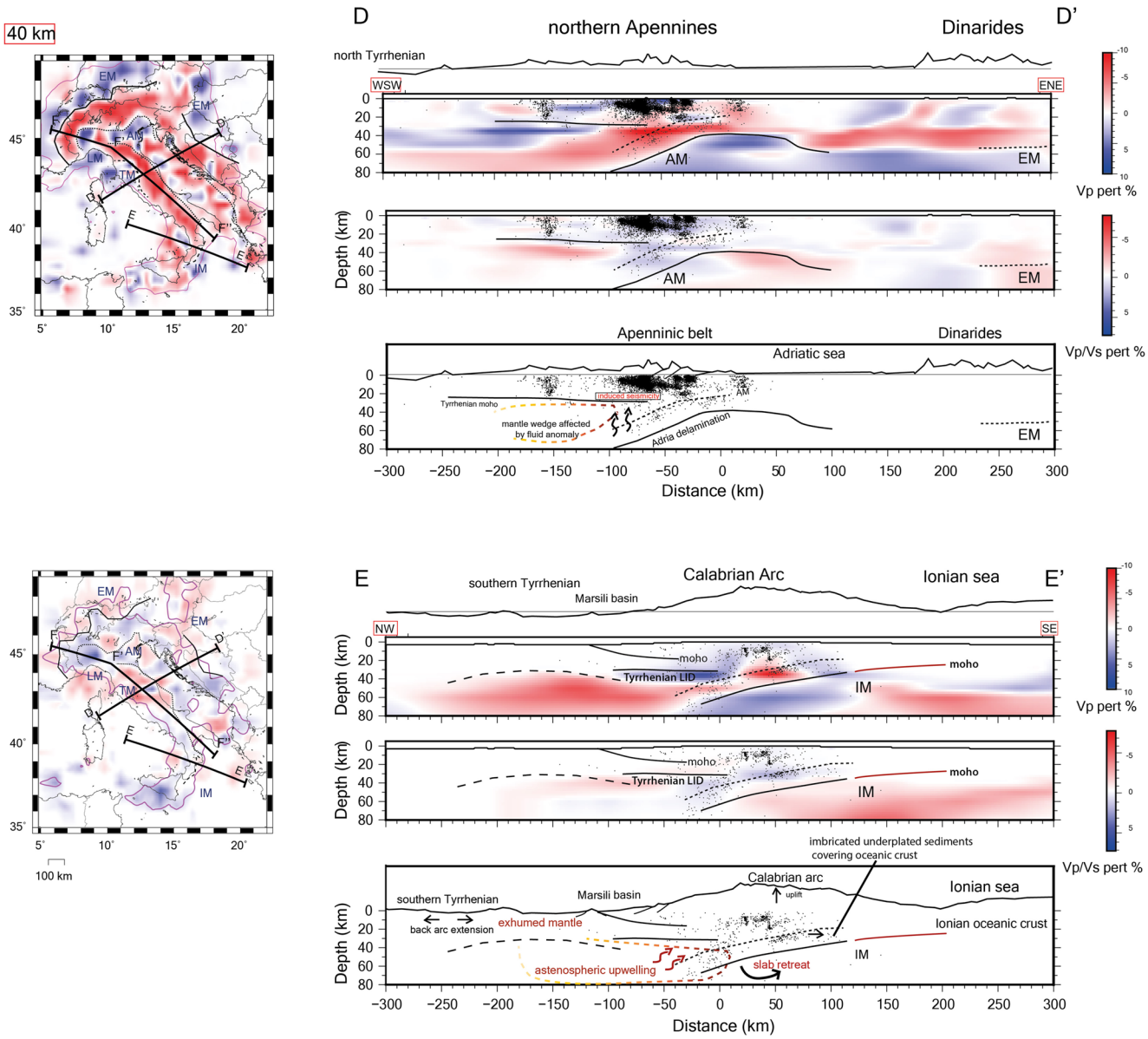

Figure 9. On the left, the *Vp* and *Vp*/*Vs* layers at a depth of 40 km with the traces of the sections (black lines) shown on the right. On the top, the tomographic section along (D–D′) the Northern Apennines and its corresponding geological sketch. On the bottom are the tomographic and interpretation sections along the Calabrian arc (E–E′). Black lines indicate the location of the Adriatic (AM), European (EM), Ligurian (LM), Tyrrhenian (TM), and Ionian lithospheric mantle (IM), whereas dotted lines indicate a position that is not highly constrained.

Below Dora Maira the mantle wedge reaches lower P velocities (<7 km/s) in both models that may suggest a serpentinized mantle (Malusà et al., 2021). In addition, the European and Adriatic Moho depths match well with Solarino et al. (2018) and with receiver function analysis (Monna et al., 2022). In particular, the Adriatic Moho appears to be consistent in depth and geometry, while the European Moho is consistent only to a depth of 40 km below the western Alps. Monna et al. (2022) interpreted the Moho geometry as a slab detachment, while we do not observe features in contrast with the continuous subduction of the European lithosphere (Figures 7 and 8a).

5. Geodynamic Inferences

Tomographic images yield drawing the lateral extent of the European, Adria and Ionian lithospheres through the entire region, allowing the deciphering of processes and plate interaction.

5.1. From Western to Eastern Alps: The European Lithospheric Underthrusting

A widely debated question concerns the polarity of subduction beneath the Alpine chain (Handy et al., 2015; Schmid et al., 2013; Ustaszewski et al., 2008). Teleseismic tomography concurred to animate this topic (Handy et al., 2021; Lippitsch, 2003; Piromallo & Morelli, 2003; Zhao et al., 2016) following the original suggestion of a change in slab polarity, where the southward European subduction switched to a northward Adria subduction, from west to east. To define the 3D geometry of the lithosphere structure below the different sectors of the Alpine chain (western, central, eastern) we draw three orogen-perpendicular cross sections (Figure 8). Our model reveals a lateral continuity of the underthrusting European mantle lithosphere (EM in Figure 8) along the entire belt, while teleseismic models have revealed a lateral interruption of the high velocity anomalies at depths greater than 120 km, with a switch between the central and eastern sectors of the chain (Kästle et al., 2020; Koulakov et al., 2009; Lippitsch, 2003; Mitterbauer et al., 2011; Zhao et al., 2016). In the western Alps (section A–A′ in Figure 8) the slab is well represented by a pair of low and high *Vp* anomalies, from 30 to 80 km, dipping southward under the Adriatic plate, associated with the subducting European lower crust and upper lithospheric mantle. The high *Vp* anomaly is in continuity with deep positive anomalies defined by teleseismic models (Giacomuzzi et al., 2011; Koulakov et al., 2009; Lyu et al., 2017; Paffrath et al., 2021; Zhao et al., 2016). Below a depth of about 60 km, the switch from low to high *Vp* suggests the eclogitization of the subducting lower crust (Christensen, 1996; among others). Evidence of this process is the high *Vp*/*Vs* anomaly in the mantle wedge representing the volume of hydrated mantle during eclogitization (Reynard, 2013). Similar high *Vp*/*Vs* in the wedge has been reported by local models (Malusà et al., 2021; Solarino et al., 2018). The Adriatic mantle lithosphere (~35 km) is clearly evidenced by high *Vp* anomalies, appearing locally flexed under the Apennines (Figure 8). The European underthrusting lithosphere is unequivocal (Figures 7 and 8) and the slab continuous and attached (Zhao et al., 2016) on the contrary of past tomographic studies (Kästle et al., 2018; Lippitsch, 2003) and receiver functions analysis (Monna et al., 2022), supportive of a shallow detachment of the European lithosphere. In the central Alps (section B–B′ in Figure 8), the plate geometry is similar to the western sector, with the EM dipping toward the south, below AM, and a central low *Vp* and high *Vp*/*Vs* volume that spread to the entire mountain roots. In the eastern Alps (section C–C' in Figure 8), we draw a section perpendicular to the EM anomaly, with a direction that is optimal to highlight the structure and geometry of the Alpine lithosphere (following Kästle et al., 2020). We observe the S-dipping pair of high and low *Vp* anomalies, attributable to the European lithosphere. The lithosphere structure does not evidence or clarify the eventual change in slab polarity, supporting the continuity of the European underthrusting (Koulakov et al., 2009; Mitterbauer et al., 2011; Zhao et al., 2016). Our results are consistent with either the scenarios I in Kästle et al. (2020), where Europe is underthrusting, or with a delamination of Adria that followed the break-off of the European slab (see also Giacomuzzi et al., 2012). A different *Vp*/*Vs* pattern observed on top of the high *Vp* mantle permits distinguishing between the European (low *Vp*/*Vs*) and Adria (high *Vp*/*Vs*) lithosphere (see section C–C′ in Figure 8). This pattern can be related to a strong hydration of the mantle top (Christensen, 1996) generated by the delamination of the Adria lithosphere. We observe that the low *Vp* anomaly at 40 and 50 km that follows the entire Alps belt spread to the east, suggesting a lateral extrusion of the accreted lithosphere after the stop of the subduction, consistent with the rotation identified by GNSS velocities (Serpelloni et al., 2022).

5.2. Delamination Versus Subduction Retreat: The Northern Apennines and Ionian Cases

The descent of the Adria plate below the Northern Apennines and the Dinarides is coherently defined by the distribution of intermediate depth earthquakes and velocity anomalies (section D–D′ in Figure 9). Anyway, since the signature of a continuous Adria slab beneath the Apennines is missing and should be recovered by our data (Figure 4), we argue that the underthrusting of the Adria mantle lithosphere is restricted to some specific portions of the orogen. The dominant feature is a low *Vp* mantle at depth below 40 km, suggestive of a spread lithospheric delamination. In the Apennines, seismicity occurs in the uppermost 15–20 km of the crust characterized by high *Vp*/*Vs* and weak positive/negative *Vp* anomalies. This region is confined downward by a strong low-*Vp*, high *Vp*/*Vs* anomaly, evidencing a vigorous dehydration process of the under-thrusting hydrated lower crust. On top of it, along the Tyrrhenian side of the belt, the shallower Tyrrhenian Moho is defined by an abrupt transition from high (above the Moho) to low *Vp*/*Vs* values, corresponding to a positive *Vp* jump below 20–30 km, consistent with the average depth observed by regional models (Spada et al., 2013). Seismicity and velocity patterns depict delamination of the Adria lithosphere, during which slices of continental crust, felsic and granulitic peeled off and replaced by sub-lithospheric mantle, composing part of the deep low *Vp* anomaly. The low *Vp* mantle wedge is coupled

with a high *Vp*/*Vs* anomaly coherent with fluid release from the under-thrusted materials (Piccinini et al., 2010). Fluid up-welling toward crustal depths could be responsible for the reactivation of normal faults, coherently with the extensional and uplift rate of ∼2–3 mm/yr reported by GPS data (Serpelloni et al., 2022). The very low *Vp*/*Vs* beneath the Tyrrhenian Moho (i.e., high *Vs*) suggests that the delamination was not accompanied by a significant asthenospheric upwelling in this region (Chiarabba et al., 2014). The high *Vp*/*Vs* beneath the belt supports the existence of a circuit of fluids that follows the retreat of the continental lithosphere and supports the dynamic topography of the belt. A slightly different pattern is observed in the southern Tyrrhenian area, where the high *Vp*, low *Vp*/*Vs* (IM) subducts beneath the Calabrian arc and the Tyrrhenian Moho (section E–E′ Figure 8). This anomaly is fully consistent with deeper slab-related positive anomalies identified by tomographic studies (Di Stefano et al., 2009; Piromallo & Morelli, 2003). Distinctive of our model is the reconnaissance of low *Vp*, high *Vp*/*Vs* anomalies on top of the Ionian lithosphere and under the mountain belt. We associate this feature with imbricated underplated and fluid-rich metasediments (Christensen, 1996) that are sandwiched between the Calabrian nappes and the subducting Ionian oceanic crust. This interpretation is coherent with a remarkable low-*Vs* zone inferred between 20 and 30 km depth from Receiver Function analysis (Agostinetti & Amato, 2009). A second significant feature revealed here is the broad and strong low *Vp* present in the Tyrrhenian area (Manu-Marfo et al., 2019) following the opening of the Marsili back-arc basin, which was accompanied by mantle exhumation and volcanism (Magni et al., 2019; Prada et al., 2020). Intense asthenospheric upwelling and melting followed the retreat of the Ionian plate generating this widespread deep negative anomaly, as recently confirmed by surface wave tomography studies (Magrini et al., 2022). The low *Vp* anomaly is coupled with a high *Vp*/*Vs* anomaly, probably due to the presence of fluids associated with the mantle inflow from the Ionian slab edges. The lack of resolution in the offshore Ionian supports the urgency of seismic experiments to define the deep geometry of the plate interface in the trench, the rock physical properties and the potential for large earthquakes and tsunamis (Maesano et al., 2017). From the velocity model reconstructed here, we can infer that the essentially sub-horizontal Ionian lithosphere may have variable thickness or heterogeneity, as indicated by the low *Vp* anomaly at depth. The two sections highlight the difference between a delamination-supported continental subduction and a retreat of an oceanic slab. In the first, the active process is restricted in a narrow area where the delamination is ongoing with a limited asthenospheric upwelling; in the latter, deformation and magmatism spread to a hundreds-kilometer scale.

5.3. *Vp*/*Vs* Anomalies in the Uppermost Mantle: Fluids or Thermal Origin?

Temperature and composition are the main parameters influencing seismic velocities in the Earth's mantle. The sensitivity of seismic velocities varies at different depths, while temperatures are thought to play a key role at upper mantle depths (Piccinini et al., 2010; Trampert et al., 2001). The reduction in Vs and increase in *Vp*/*Vs* could be attributed either to the presence of water related to hydration processes (Christensen, 1996; Shito et al., 2006) or to partial melts (Hammond & Humphreys, 2000).

Although it is often difficult to discern to which extent velocity anomalies reflect composition rather than thermal anomalies (Cammarano et al., 2003), the joint interpretation of *Vp* and *Vp*/*Vs* models is helpful (Giacomuzzi et al., 2012).

Beneath the Alps and northern Apennines, the low *Vp*, high *Vp*/*Vs* anomaly at 40–60 km depth (Figure 10) is consistent with a strong hydration of the mantle wedge generated by the delamination of the continental lithosphere. Along the Apennines, we observe a transition from a sector where the Moho doubling is evident (X = 400–650 km in sections of Figure 10) to a flat Adria Moho in the south (X = 850–1,150 km), while the uppermost mantle is remarkably slow in the central portion (Vp = 7.5 km/s). This pattern suggests that the delamination process of the Adria lithosphere proceeded with different retreat velocity along the belt generating an irregular geometry, in agreement with a different level of subduction maturity hypothesized also by velocity reduction in the mantle beneath the LAB defined by S-Receiver Function (Miller & Agostinetti, 2012). Mantle substitution generated during the delamination dynamically sustains the belt topography.

Conversely, the wide low-*Vp* mantle anomaly in the southern Tyrrhenian back-arc region (Manu-Marfo et al., 2019) can be interpreted as due to a thermal anomaly of the upwelling asthenosphere generated by the slab retreat (Figure 9).

6. Conclusion

We provide new insights into the geometry of the Alpine and Apennine belt systems, the compositional and thermal state of the lithospheric mantle, and the lateral (i.e., temporal) heterogeneity of the delamination and

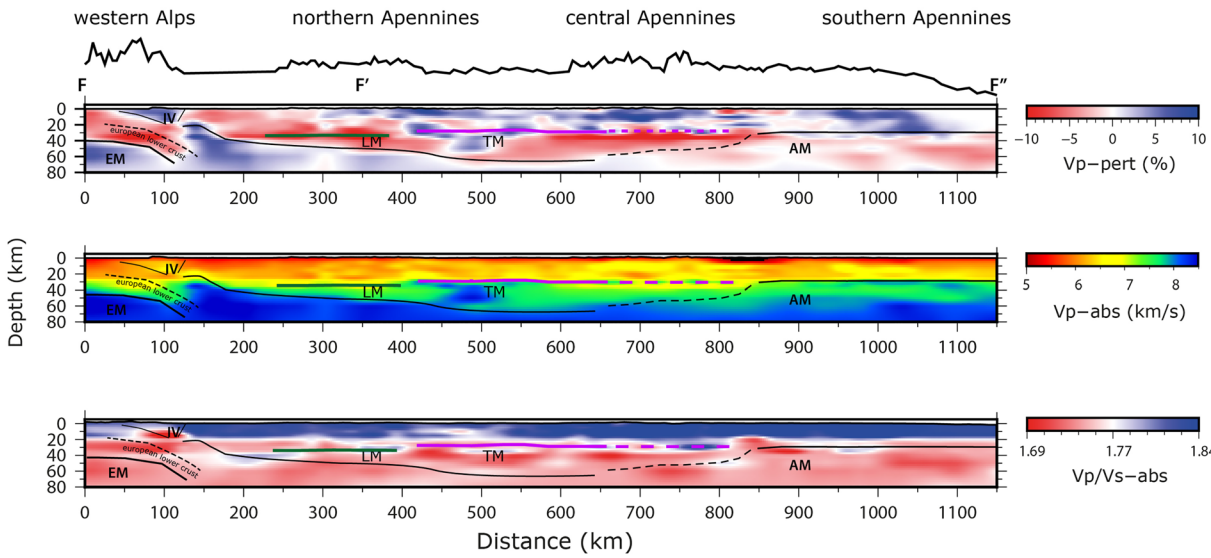

Figure 10. Cross sections along the western Alps-Apennines (perturbation model *Vp* at top, absolute values of *Vp* and *Vp*/*Vs*, in center and bottom respectively). The black lines indicate the location of the European and the Adriatic moho, the purple line the Tyrrhenian moho. Dotted lines indicate a position that is not highly constrained. IV: Ivrea Body, LM: Ligurian lithospheric Mantle, EM: European lithospheric Mantle, AM: Adriatic lithospheric Mantle.

subduction process beneath the central Mediterranean area. New *Vp* and *Vp*/*Vs* models were computed by inverting a huge amount of seismic data recorded continuously from the densest seismic array ever installed before comprising permanent and temporary seismic stations. The inversion of travel times of refracted waves (Pn and Sn) up to an epicentral distance of 1,000 km, yield high resolution and homogeneous information on the lower crust and lithospheric mantle of the Adriatic and European plates with unprecedented consistency throughout the central Mediterranean area. The layers and tomographic sections shed light on the compositional, thermal, and velocity heterogeneities that control the subduction processes beneath the Alpine and Apennine ranges. We observe a continuous underthrusting of the European lithosphere below the entire Alpine chain. We find no gaps below the Western Alps and not a clear reversal of plate polarity in the eastern sector. The overlap of positive anomalies at 60–80 km depth by one side supports the continuity of the European underthrusting, but inhibits further distinction on the nature of the subducting slab (European vs. Adriatic). A future advancement could be the computation of a teleseismic model after stripping the crustal contribution from this model. A final remark is on the interpretation of *Vp* and *Vp*/*Vs* models, with new constraints on the fluid release processes that occurred during the descent of the Adriatic lithosphere and the dehydration of subducted crustal sediments forming large sack of fluids beneath the mountain belts, the release of which is coupled with extensional deformation.

Conflict of Interest

The authors declare no conflicts of interest relevant to this study.

Data Availability Statement

Seismograms analyzed in this study have been recorded in the frame of AlpArray project by the temporary array and the permanent networks that contributed to the European program (AlpArraySeismicNetwork, 2015; Hetényi et al., 2018; INGV Seismological Data Centre, 1997). Earthquake data of Italian seismicity have been provided by Istituto Nazionale di Geofisica e Vulcanologia (INGV) and can retrieved in the EIDA database (http://eida.rm.ingv.it). Figures were made using Generic Mapping Tools (GMT) software (Wessel et al., 2013).

Acknowledgments
We thank the anonymous reviewers for comments and suggestions that improved the quality and robustness of the work. The authors would like to thank to the AlpArray Seismic Network Team: György Hetényi, Rafael Abreu, Ivo Allegretti, Maria-Theresia Apoloner, Coralie Aubert, Simon Besançon, Maxime Bès De Berc, Götz Bokelmann, Didier Brunel, Marco Capello, Martina Čarman, Adriano Cavaliere, Jérôme Chèze, Claudio Chiarabba, John Clinton, Glenn Cougoulat, Wayne C. Crawford, Luigia Cristiano, Tibor Czifra, Ezio D'alema, Stefania Danesi, Romuald Daniel, Anke Dannowski, Iva Dasović, Anne Deschamps, Jean-Xavier Dessa, Cécile Doubre, Sven Egdorf, Ethz-Sed Electronics Lab, Tomislav Fiket, Kasper Fischer, Wolfgang Friederich, Florian Fuchs, Sigward Funke, Domenico Giardini, Aladino Govoni, Zoltán Gráczer, Gidera Gröschl, Stefan Heimers, Ben Heit, Davorka Herak, Marijan Herak, Johann Huber, Dejan Jarić, Petr Jedlička, Yan Jia, Hélène Jund, Edi Kissling, Stefan Klingen, Bernhard Klotz, Petr Kolínský, Heidrun Kopp, Michael Korn, Josef Kotek, Lothar Kühne, Krešo Kuk, Dietrich Lange, Jürgen Loos, Sara Lovati, Deny Malengros, Lucia Margheriti, Christophe Maron, Xavier Martin, Marco Massa, Francesco Mazzarini, Thomas Meier, Laurent Métral, Irene Molinari, Milena Moretti, Anna Nardi, Jurij Pahor, Anne Paul, Catherine Péquegnat, Daniel Petersen, Damiano Pesaresi, Davide Piccinini, Claudia Piromallo, Thomas Plenefisch, Jaroslava Plomerová, Silvia Pondrelli, Snježan Prevolnik, Roman Racine, Marc Régnier, Miriam Reiss, Joachim Ritter, Georg Rümpker, Simone Salimbeni, Marco Santulin, Werner Scherer, Sven Schippkus, Detlef Schulte-Kortnack, Vesna Šipka, Stefano Solarino, Daniele Spallarossa, Kathrin Spieker, Josip Stipčević, Angelo Strollo, Bálint Süle, Gyöngyvér Szanyi, Eszter Szűcs, Christine Thomas, Martin Thorwart, Frederik Tilmann, Stefan Ueding, Massimiliano Vallocchia, Luděk Vecsey, René Voigt, Joachim Wassermann, Zoltán Wéber, Christian Weidle, Viktor Wesztergom, Gauthier Weyland, Stefan Wiemer, Felix Wolf, David Wolyniec, Thomas Zieke, Mladen Živčić and Helena Žlebčíková. For further information regarding the team, please visit the link http://www.alparray.ethz.ch. Open Access Funding provided by Istituto Nazionale di Geofisica e Vulcanologia within the CRUI-CARE Agreement.

References

Agostinetti, N. P., & Amato, A. (2009). Moho depth and Vp/Vs ratio in peninsular Italy from teleseismic receiver functions. *Journal of Geophysical Research*, *114*(B6), 1–17. https://doi.org/10.1029/2008JB005899

AlpArray Seismic Network. (2014). *Eastern Alpine Seismic Investigation (EASI) - AlpArray complimentary experiment*. AlpArray Working Group. Retrieved from http://networks.seismo.ethz.ch/networks/xt/

AlpArraySeismicNetwork. (2015). *AlpArray Seismic Network (AASN) temporary component*. AlpArray Working Group.

Bally, A. W. (1987). Balanced sections and seismic reflection profiles across the central Apennines.

Bezacier, L., Reynard, B., Bass, J. D., Sanchez-Valle, C., & Van de Moortèle, B. (2010). Elasticity of antigorite, seismic detection of serpentinites, and anisotropy in subduction zones. *Earth and Planetary Science Letters*, *289*(1–2), 198–208. https://doi.org/10.1016/j.epsl.2009.11.009

Buttinelli, M., Pezzo, G., Valoroso, L., De Gori, P., & Chiarabba, C. (2018). Tectonics inversions, fault segmentation, and triggering mechanisms in the central Apennines normal fault system: Insights from high-resolution velocity models. *Tectonics*, *37*(11), 4135–4149. https://doi.org/10.1029/2018tc005053

Cammarano, F., Goes, S., Vacher, P., & Giardini, D. (2003). Inferring upper-mantle temperatures from seismic velocities. *Physics of the Earth and Planetary Interiors*, *138*(3–4), 197–222. https://doi.org/10.1016/s0031-9201(03)00156-0

Carminati, E., Lustrino, M., & Doglioni, C. (2012). Geodynamic evolution of the central and Western mediterranean: Tectonics vs. igneous petrology constraints. *Tectonophysics*, *579*, 173–192. https://doi.org/10.1016/j.tecto.2012.01.026

Chiarabba, C., De Gori, P., & Mele, F. M. (2015). Recent seismicity of Italy: Active tectonics of the central Mediterranean region and seismicity rate changes after the Mw 6.3 L'Aquila earthquake. *Tectonophysics*, *638*(1), 82–93. https://doi.org/10.1016/j.tecto.2014.10.016

Chiarabba, C., Giacomuzzi, G., Bianchi, I., Agostinetti, N. P., & Park, J. (2014). From underplating to delamination-retreat in the Northern Apennines. *Earth and Planetary Science Letters*, *403*, 108–116. https://doi.org/10.1016/j.epsl.2014.06.041

Christensen, N. I. (1996). Poisson's ratio and crustal seismology. *Journal of Geophysical Research*, *101*(B2), 3139–3156. https://doi.org/10.1029/95jb03446

Christensen, N. I. (2004). Serpentinites, peridotites, and seismology. *International Geology Review*, *46*(9), 795–816.

Christensen, N. I., & Mooney, W. D. (1995). Seismic velocity structure and composition of the continental crust: A global view. *Journal of Geophysical Research: Solid Earth*, *100*(B6), 9761–9788. https://doi.org/10.1029/95jb00259

Di Stefano, R., & Ciaccio, M. G. (2014). The lithosphere and asthenosphere system in Italy as inferred from the Vp and vs 3D velocity model and Moho map. *Journal of Geodynamics*, *82*, 16–25. https://doi.org/10.1016/j.jog.2014.09.006

Di Stefano, R., Kissling, E., Chiarabba, C., Amato, A., & Giardini, D. (2009). Shallow subduction beneath Italy: Three-dimensional images of the Adriatic-European-Tyrrhenian lithosphere system based on high-quality P wave arrival times. *Journal of Geophysical Research: Solid Earth*, *114*(5), 1–17. https://doi.org/10.1029/2008JB005641

Diehl, T., Husen, S., Kissling, E., & Deichmann, N. (2009). High-resolution 3-D P-wave model of the Alpine crust. *Geophysical Journal International*, *179*(2), 1133–1147. https://doi.org/10.1111/j.1365-246X.2009.04331.x

Eberhart-Phillips, D., & Reyners, M. (1997). Continental subduction and three-dimensional crustal structure: The northern south island, New Zealand. *Journal of Geophysical Research: Solid Earth*, *102*(B6), 11843–11861. https://doi.org/10.1029/96jb03555

Faccenna, C., & Becker, T. W. (2010). Shaping mobile belts by small-scale convection. *Nature*, *465*(7298), 602–605. https://doi.org/10.1038/nature09064

Faccenna, C., Becker, T. W., Auer, L., Billi, A., Boschi, L., Brun, J. P., et al. (2014). Mantle dynamics in the mediterranean. *Reviews of Geophysics*, *52*(3), 283–332. https://doi.org/10.1002/2013rg000444

Giacomuzzi, G., Chiarabba, C., & De Gori, P. (2011). Linking the Alps and Apennines subduction systems: New constraints revealed by high-resolution teleseismic tomography. *Earth and Planetary Science Letters*, *301*(3–4), 531–543. https://doi.org/10.1016/j.epsl.2010.11.033

Giacomuzzi, G., Civalleri, M., De Gori, P., & Chiarabba, C. (2012). A 3D vs model of the upper mantle beneath Italy: Insight on the geodynamics of central Mediterranean. *Earth and Planetary Science Letters*, *335–336*, 105–120. https://doi.org/10.1016/j.epsl.2012.05.004

Grevemeyer, I., Ranero, C. R., & Ivandic, M. (2018). Structure of oceanic crust and serpentinization at subduction trenches. *Geosphere*, *14*(2), 395–418. https://doi.org/10.1130/ges01537.1

Hammond, W. C., & Humphreys, E. D. (2000). Upper mantle seismic wave velocity: Effects of realistic partial melt geometries. *Journal of Geophysical Research: Solid Earth*, *105*(B5), 10975–10986. https://doi.org/10.1029/2000jb900041

Handy, M., Schmid, S., Paffrath, M., & Friederich, W. (2021). European tectosphere and slabs beneath the greater Alpine area – Interpretation of mantle structure in the Alps-Apennines-Pannonian region from teleseismic Vp studies. *Solid Earth Discussions*(May), 1–61. https://doi.org/10.5194/se-2021-49

Handy, M., Ustaszewski, K., & Kissling, E. (2015). Reconstructing the Alps–Carpathians–Dinarides as a key to understanding switches in subduction polarity, slab gaps and surface motion. *International Journal of Earth Sciences*, *104*(1), 1–26. https://doi.org/10.1007/s00531-014-1060-3

Hetényi, G., Molinari, I., Clinton, J., Bokelmann, G., Bondár, I., Crawford, W. C., et al. (2018). The AlpArray seismic network: A large-scale European experiment to image the alpine orogen. *Surveys in Geophysics*, *39*(5), 1009–1033. https://doi.org/10.1007/s10712-018-9472-4

Improta, L., Bagh, S., De Gori, P., Valoroso, L., Pastori, M., Piccinini, D., et al. (2017). Reservoir structure and wastewater-induced seismicity at the Val d'Agri oilfield (Italy) shown by three-dimensional Vp and Vp/Vs local earthquake tomography. *Journal of Geophysical Research: Solid Earth*, *122*(11), 9050–9082. https://doi.org/10.1002/2017jb014725

Improta, L., Bonagura, M., Capuano, P., & Iannaccone, G. (2003). An integrated geophysical investigation of the upper crust in the epicentral area of the 1980, ms = 6.9, Irpinia earthquake (southern Italy). *Tectonophysics*, *361*(1–2), 139–169. https://doi.org/10.1016/s0040-1951(02)00588-7

INGV Seismological Data Centre. (1997). *Rete Sismica Nazionale (RSN)*. Istituto Nazionale di Geofisica e Vulcanologia (INGV). http://doi.org/10.13127/SD/X0FXnH7QfY

Kästle, E. D., El-Sharkawy, A., Boschi, L., Meier, T., Rosenberg, C., Bellahsen, N., et al. (2018). Surface wave tomography of the alps using ambient-noise and earthquake phase velocity measurements. *Journal of Geophysical Research: Solid Earth*, *123*(2), 1770–1792. https://doi.org/10.1002/2017JB014698

Kästle, E. D., Rosenberg, C., Boschi, L., Bellahsen, N., Meier, T., & El-Sharkawy, A. (2020). Slab break-offs in the alpine subduction zone. *International Journal of Earth Sciences*, *109*(2), 587–603. https://doi.org/10.1007/s00531-020-01821-z

Koulakov, I., Kaban, M. K., Tesauro, M., & Cloetingh, S. (2009). P- and S-velocity anomalies in the upper mantle beneath Europe from tomographic inversion of ISC data. *Geophysical Journal International*, *179*(1), 345–366. https://doi.org/10.1111/j.1365-246X.2009.04279.x

Lévêque, J.-J., Rivera, L., & Wittlinger, G. (1993). On the use of the checker-board test to assess the resolution of tomographic inversions. *Geophysical Journal International*, *115*(1), 313–318. https://doi.org/10.1111/j.1365-246X.1993.tb05605.x

Lippitsch, R. (2003). Upper mantle structure beneath the Alpine orogen from high-resolution teleseismic tomography. *Journal of Geophysical Research*, *108*(B8), 2376. https://doi.org/10.1029/2002jb002016

Lyu, C., Pedersen, H. A., Paul, A., Zhao, L., Solarino, S., Aubert, C., & Zhu, R. (2017). Shear wave velocities in the upper mantle of the Western Alps: New constraints using array analysis of seismic surface waves. *Geophysical Journal International*, *210*(1), 321–331. https://doi.org/10.1093/gji/ggx166

Maesano, F. E., Tiberti, M. M., & Basili, R. (2017). The Calabrian Arc: Three-dimensional modelling of the subduction interface. *Scientific Reports*, *7*(1), 1–15. https://doi.org/10.1038/s41598-017-09074-8

Magni, V., Király, Á., Evolution, E., & Ceed, D. (2019). What is delamination? Subducting plate delamination. (December), 1–8.

Magrini, F., Diaferia, G., El-Sharkawy, A., Cammarano, F., vanDer Meijde, M., Meier, T., & Boschi, L. (2022). Surface-wave tomography of the Central-Western Mediterranean: New insights into the Liguro-Provençal and Tyrrhenian basins. *Journal of Geophysical Research: Solid Earth*, *127*(3), e2021JB023267. https://doi.org/10.1029/2021jb023267

Malusà, M. G., Guillot, S., Zhao, L., Paul, A., Solarino, S., Dumont, T., et al. (2021). The deep structure of the alps based on the CIFALPS seismic experiment: A synthesis. *Geochemistry, Geophysics, Geosystems*, *22*(3), 1–42. https://doi.org/10.1029/2020GC009466

Manu-Marfo, D., Aoudia, A., Pachhai, S., & Kherchouche, R. (2019). 3D shear wave velocity model of the crust and uppermost mantle beneath the Tyrrhenian basin and margins. *Scientific Reports*, *9*(1), 1–10. https://doi.org/10.1038/s41598-019-40510-z

Menichelli, I., De Gori, P., Lucente, F. P., Improta, L., Valoroso, L., Baccheschi, P., et al. (2022). Minimum 1D VP and VP/VS models and hypocentral determinations in the central mediterranean area. *Seismological Research Letters*, *06*(5), 2670–2685. https://doi.org/10.1785/0220220079

Michelini, A., & McEvilly, T. (1991). Seismological studies at Parkfield. I. Simultaneous inversion for velocity structure and hypocenters using cubic B-splines parameterization. *Bulletin of the Seismological Society of America*, *81*(2), 524–552.

Miller, M. S., & Agostinetti, N. P. (2012). Insights into the evolution of the Italian lithospheric structure from s receiver function analysis. *Earth and Planetary Science Letters*, *345*, 49–59. https://doi.org/10.1016/j.epsl.2012.06.028

Mitterbauer, U., Behm, M., Brückl, E., Lippitsch, R., Guterch, A., Keller, G. R., et al. (2011). Shape and origin of the East-Alpine slab constrained by the ALPASS teleseismic model. *Tectonophysics*, *510*(1–2), 195–206. https://doi.org/10.1016/j.tecto.2011.07.001

Monna, S., Montuori, C., Frugoni, F., Piromallo, C., Vinnik, L., & AlpArray Group. (2022). Moho and LAB across the Western alps (Europe) from p and s receiver function analysis. *Journal of Geophysical Research: Solid Earth*, *127*(10), e2022JB025141. https://doi.org/10.1029/2022jb025141

Nocquet, J.-M. (2012). Present-day kinematics of the mediterranean: A comprehensive overview of GPS results. *Tectonophysics*, *579*, 220–242. https://doi.org/10.1016/j.tecto.2012.03.037

Paffrath, M., Friederich, W., Schmid, S. M., Handy, M. R., & AlpArray and AlpArray-Swath D Group. (2021). Imaging structure and geometry of slabs in the greater alpine area–a P-wave travel-time tomography using AlpArray seismic network data. *Solid Earth*, *12*(11), 2671–2702. https://doi.org/10.5194/se-12-2671-2021

Piccinini, D., Di Bona, M., Lucente, F. P., Levin, V., & Park, J. (2010). Seismic attenuation and mantle wedge temperature in the northern Apennines subduction zone (Italy) from teleseismic body wave spectra. *Journal of Geophysical Research: Solid Earth*, *115*(B9), B09309. https://doi.org/10.1029/2009jb007180

Piromallo, C., & Morelli, A. (2003). P wave tomography of the mantle under the Alpine-Mediterranean area. *Journal of Geophysical Research: Solid Earth*, *108*(B2), 1–23. https://doi.org/10.1029/2002jb001757

Prada, M., Ranero, C. R., Sallarès, V., Grevemeyer, I., de Franco, R., Gervasi, A., & Zitellini, N. (2020). The structure of Mediterranean arcs: New insights from the Calabrian Arc Subduction System. *Earth and Planetary Science Letters*, *548*, 116480. https://doi.org/10.1016/j.epsl.2020.116480

Reynard, B. (2013). Serpentine in active subduction zones. *Lithos*, *178*, 171–185. https://doi.org/10.1016/j.lithos.2012.10.012

Salimbeni, S., Pondrelli, S., Margheriti, L., Park, J., & Levin, V. (2008). Sks splitting measurements beneath northern Apennines region: A case of oblique trench-retreat. *Tectonophysics*, *462*(1–4), 68–82. https://doi.org/10.1016/j.tecto.2007.11.075

Scafidi, D., & Solarino, S. (2012). Can local earthquake tomography settle the matter about subduction in the Northern and Central Apennines? Response from a new high resolution P velocity and Vp/Vs ratio 3-D model. *Tectonophysics*, *554*, 63–73. https://doi.org/10.1016/j.tecto.2012.06.007

Scafidi, D., Solarino, S., & Eva, C. (2009). P wave seismic velocity and Vp/Vs ratio beneath the Italian peninsula from local earthquake tomography. *Tectonophysics*, *465*(1–4), 1–23. https://doi.org/10.1016/j.tecto.2008.07.013

Schmid, S. M., Fügenschuh, B., Cavazza, I., Roure, F., & Spakman, W. (2004). Three lithospheric transects across the Alps and their forelands explanatory text and figures in PDF-format (regarding the transects see the last three pages of this PDF file!). The TRANSMED : Atlas: The Mediterranean Region from Crust to Mantle.

Schmid, S. M., Scharf, A., Handy, M. R., & Rosenberg, C. L. (2013). The Tauern window (Eastern Alps, Austria): A new tectonic map, with cross-sections and a tectonometamorphic synthesis. *Swiss Journal of Geosciences*, *106*(1), 1–32. https://doi.org/10.1007/s00015-013-0123-y

Serpelloni, E., Cavaliere, A., Martelli, L., Pintori, F., Anderlini, L., Borghi, A., et al. (2022). Surface velocities and strain-rates in the Euro-Mediterranean region from massive GPS data processing. *Frontiers of Earth Science*, *10*. https://doi.org/10.3389/feart.2022.907897

Shito, A., Karato, S.-I., Matsukage, K. N., Nishihara, Y., Jacobsen, S., & Van Der Lee, S. (2006). Towards mapping the three-dimensional distribution of water in the upper mantle from velocity and attenuation tomography. *Geophysical Monograph-American Geophysical Union*, *168*, 225.

Solarino, S., Malusà, M. G., Eva, E., Guillot, S., Paul, A., Schwartz, S., et al. (2018). Mantle wedge exhumation beneath the Dora-Maira (U)HP dome unravelled by local earthquake tomography (Western Alps). *Lithos*, *296*, 623–636. https://doi.org/10.1016/j.lithos.2017.11.035

Spada, M., Bianchi, I., Kissling, E., Agostinetti, N. P., & Wiemer, S. (2013). Combining controlled-source seismology and receiver function information to derive 3-D Moho topography for Italy. *Geophysical Journal International*, *194*(2), 1050–1068. https://doi.org/10.1093/gji/ggt148

Thomson, S. N., Brandon, M. T., Reiners, P. W., Zattin, M., Isaacson, P. J., & Balestrieri, M. L. (2010). Thermochronologic evidence for orogen-parallel variability in wedge kinematics during extending convergent orogenesis of the northern apennines, Italy. *Bulletin*, *122*(7–8), 1160–1179. https://doi.org/10.1130/b26573.1

Toomey, D., & Foulger, G. (1989). Tomographic inversion of local earthquake data from the Hengill-Grensdalur Central Volcano complex, Iceland. *Journal of Geophysical Research: Solid Earth*, *94*(B12), 17497–17510. https://doi.org/10.1029/jb094ib12p17497

Trampert, J., Vacher, P., & Vlaar, N. (2001). Sensitivities of seismic velocities to temperature, pressure and composition in the lower mantle. *Physics of the Earth and Planetary Interiors*, *124*(3), 255–267. https://doi.org/10.1016/S0031-9201(01)00201-1

Trippetta, F., Collettini, C., Vinciguerra, S., & Meredith, P. (2010). Laboratory measurements of the physical properties of triassic evaporites from central Italy and correlation with geophysical data. *Tectonophysics*, *492*(1–4), 121–132. https://doi.org/10.1016/j.tecto.2010.06.001

Ustaszewski, K., Schmid, S. M., FüGENSCHUH, B., Tischler, M., Kissling, E., & Spakman, W. (2008). A map-view restoration of the Alpine-Carpathian-Dinaridic system for the early miocene. *Swiss Journal of Geosciences*, *101*(1), 273–294. https://doi.org/10.1007/s00015-008-1288-7

Wessel, P., Smith, W. H., Scharroo, R., Luis, J., & Wobbe, F. (2013). Generic mapping tools: Improved version released. *EOS, Transactions American Geophysical Union*, *94*(45), 409–410. https://doi.org/10.1002/2013eo450001

Wortel, M., & Spakman, W. (2000). Subduction and slab detachment in the Mediterranean-Carpathian region. *Science*, *290*(5498), 1910–1917. https://doi.org/10.1126/science.290.5498.1910

Zhao, L., Paul, A., Malusà, M. G., Xu, X., Zheng, T., Solarino, S., et al. (2016). Continuity of the Alpine slab unraveled by high-resolution P wave tomography. *Journal of Geophysical Research: Solid Earth*, *121*(12), 8720–8737. https://doi.org/10.1002/2016JB013310